

Preparation of Drug Nanoparticles Using a T-Junction Microchannel System

Qian-Xia Zhang^{†,‡} Li-Min Xu,[†] Yue Zhou,[†] Jie-Xin Wang,^{*,†} and Jian-Feng Chen^{†,§}

[†]State Key Laboratory of Organic—Inorganic Composites and [§]Research Center of the Ministry of Education for High Gravity Engineering and Technology, Beijing University of Chemical Technology, Beijing 100029, P.R. China

[‡]Institute of Coal Chemistry, Chinese Academy of Sciences, Taiyuan, Shanxi 030001, P.R. China

ABSTRACT: Cefuroxime axetil (CFA) drug nanoparticles were prepared by liquid antisolvent precipitation in a microchannel system with a T-shaped junction formed by a main microchannel and a branch. Isopropyl ether as the antisolvent (high flow rate) was usually passed through the main microchannel, and CFA acetone solution as the solvent (low flow rate) was injected into the branch simultaneously. The solvent diffused from the CFA acetone solution stream into the antisolvent phase, which resulted in the supersaturation of CFA and thus led to the rapid precipitation of CFA nanoparticles. The change of the injection phase from CFA acetone solution to isopropyl ether was found to have a significant effect on the formation of CFA nanoparticles owing to the different contact behavior. The morphology and size of CFA nanoparticles were characterized by scanning electronic microscopy (SEM) and particle size distribution (PSD) measurements by laser diffractometry. Furthermore, the effects of CFA acetone solution velocity, antisolvent velocity, overall velocity, and CFA concentration on the particle size and size distribution were experimentally investigated. The as-prepared CFA nanoparticles were amorphous and exhibited a higher dissolution rate than raw CFA. This work suggests that microfluidics might find wide applications in the development and optimization of drug nanoparticles in the newly emerging field of nanomedicine.

1. INTRODUCTION

The poor aqueous solubility of drug candidates presents a significant problem in drug development and related requirements such as bioavailability and a normal absorption pattern.^{1–3} A variety of strategies have emerged to address the solubility issue, such as size reduction,^{4,5} the use of surfactants,^{5–8} the formation of solid dispersions,⁹ and the transformation of crystalline drugs to an amorphous state.¹⁰ Among various strategies, reducing the drug particle size has emerged as an effective and versatile option.^{3,11–17} Complementary to traditional methods for particle size reduction is the development of the liquid antisolvent precipitation (LASP) process, which offers an attractive alternative for drug nanoparticle formation at normal temperatures and pressures with no requirements for expensive equipment and is based on the change of supersaturation caused by mixing a solution and an antisolvent.^{15–22}

In recent years, there has been tremendous development in the field of microfluidic systems.^{23,24} Microfluidic devices have been used in many fields because of their high efficiency, safety, repeatability, and facile controllability.^{25–30} Compared to conventional bulk synthesis, the ability of microfluidic systems to rapidly mix reagents, provide homogeneous reaction environments, continuously vary reaction conditions, and add reagents at precise time intervals during reaction progression has made them attractive for a myriad of applications.^{31,32} In addition, from an industrial standpoint, microfluidic reactors allow precise control of process parameters to achieve optimal conditions using very small amounts of reagents and eliminate the need to scale up a reaction.³³

The convergence of microfluidics has shown considerable promise allowing for the development of inorganic nanoparticles^{34–40} and microparticles,⁴¹ in some cases with narrow size distributions,

addressing an important challenge for their maximum exploitation. Relatively little work has been done to harness the benefits of microfluidics for the synthesis of organic nanoparticles,^{20,42–44} especially drug nanoparticles. This is particularly important in the pharmaceutical industry, as the preparation of pharmaceutical nanoparticles by bulk mixing typically lacks control over the mixing processes, which could compromise the properties of the resulting particles.^{43,44} It is well-known that the particle size and distribution of a drug have significant effects on its cellular interactions and biodistribution in the body. Also, making poorly water-soluble drugs into nanoparticles not only increases their dissolution rates but also maximizes their therapeutic effectiveness. However, the synthesis of pharmaceutical nanoparticles is still a very relevant challenge.

Cefuroxime axetil (CFA) is a poorly water-soluble drug with a high activity against Gram-positive and Gram-negative microorganisms. CFA exists in crystalline and amorphous forms, with the latter showing higher bioavailability and, therefore, being more desirable. In this work, we proposed to prepare CFA nanoparticles as a model drug by controlled antisolvent precipitation in a microchannel system with a T-shaped junction formed by a main microchannel and a branch. During the process, CFA acetone solution and isopropyl ether were used as the solvent (S) and antisolvent (AS), respectively. The as-prepared CFA nanoparticles with a tunable size and narrow size distribution could be achieved by varying various process parameters such as

Received: June 17, 2011

Accepted: November 17, 2011

Revised: November 14, 2011

Published: November 17, 2011

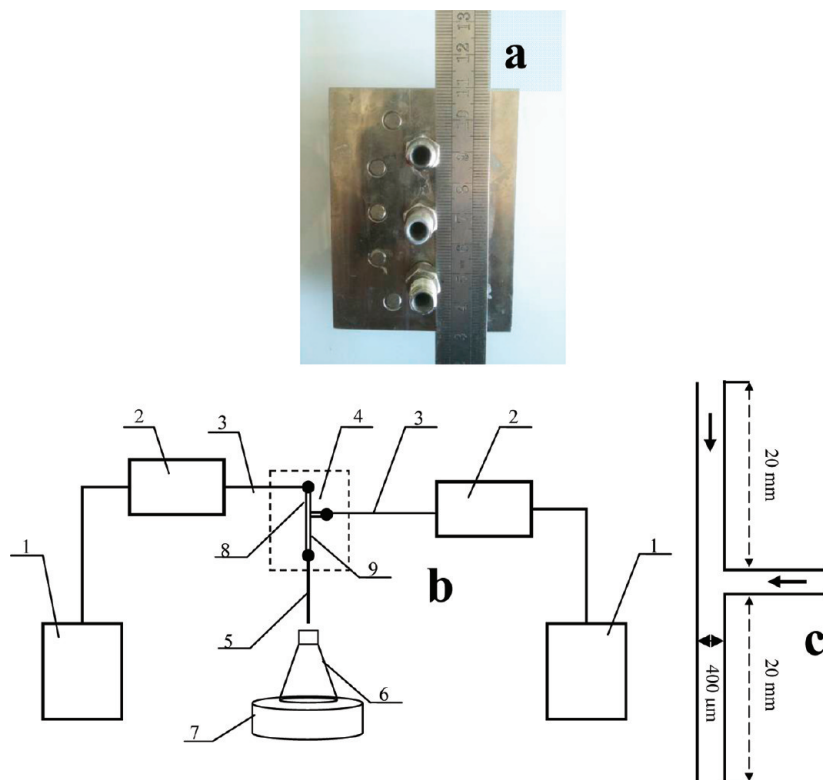


Figure 1. (a) Photograph of the TMC. (b) Schematic diagram of the overall experimental setup: (1) tank, (2) continuous nonpulsatile pumps, (3) inlet, (4) T-junction microchannel module, (5) outlet of slurry, (6) slurry container, (7) stirred collection unit, (8, 9) the TMC. (c) Schematic of the TMC section.

the flow behavior, the velocity of CFA acetone solution, the velocity of isopropyl ether, the overall velocity, and the concentration of CFA acetone solution. In particular, the effect of the injection phase at the T-shaped junction on the formation of CFA nanoparticles was investigated. The properties of the raw drug and CFA nanoparticles were also compared by scanning electronic microscopy (SEM), Fourier transform infrared (FTIR) spectroscopy, X-ray diffraction (XRD), differential scanning calorimetry (DSC), and dissolution tests.

2. EXPERIMENTAL SECTION

2.1. Materials. Raw CFA was obtained from North China Pharmaceutical Group Corporation (NCPGC) Beta Co., Ltd. Acetone, isopropyl ether (AR grade), and sodium dodecyl sulfate (SDS) were purchased from Beijing Chemical Agent Co. Water was purified to type I reagent grade by passing it through a Barnstead (Nanopure II) filtration system.

2.2. Preparation of CFA Nanoparticles. Figure 1a shows a picture of the T-shaped microchannel (TMC) used in this work, and Figure 1b schematically illustrates the overall experimental system. The system consisted of a microchannel module, two continuous nonpulsatile pumps for supplying the antisolvent and the CFA acetone solution, and a unit for collecting the CFA suspension. The TMC system was made of stainless steel, and its structure is schematically illustrated in Figure 1c. The width and depth of the TMC were 400 and 500 μm , respectively. The lengths of the inlet channel and mixing channel were both 20 mm.

The experiments were carried out as follows: Typically, raw crystalline CFA drug was first dissolved in acetone and then

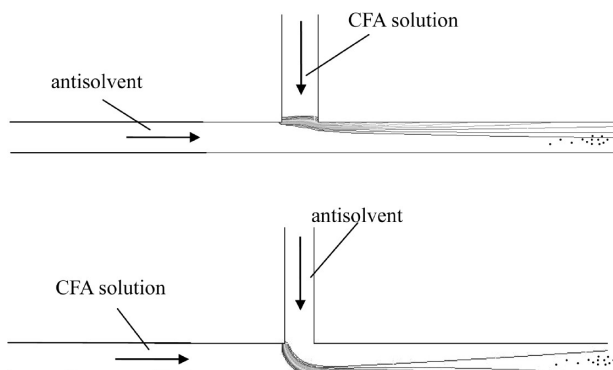


Figure 2. Schematic diagrams of the formation process of CFA nanoparticles in a TMC with different injection phases.

filtered through a 0.22- μm nylon filter to remove impurities. Afterward, CFA acetone solution and isopropyl ether were pumped into the two inlets. The rapid mixing of the two solutions took place at the T-shaped junction, and a precipitate was generated immediately. Subsequently, the effluent obtained from the outlet stream was diluted for the analysis of particle size and particle size distribution. Finally, the effluent was filtered through a 0.22- μm nylon filter, and the precipitate was dried at 40 °C under vacuum conditions to collect the drug powder for further analysis.

2.3. Characterization. The morphology of the CFA particles was visualized by scanning electron microscopy (SEM) (JEOL, JSM-6701) at 10 kV. The sample, an appropriate amount of CFA powder or a glass slide with a small drop of the suspension,

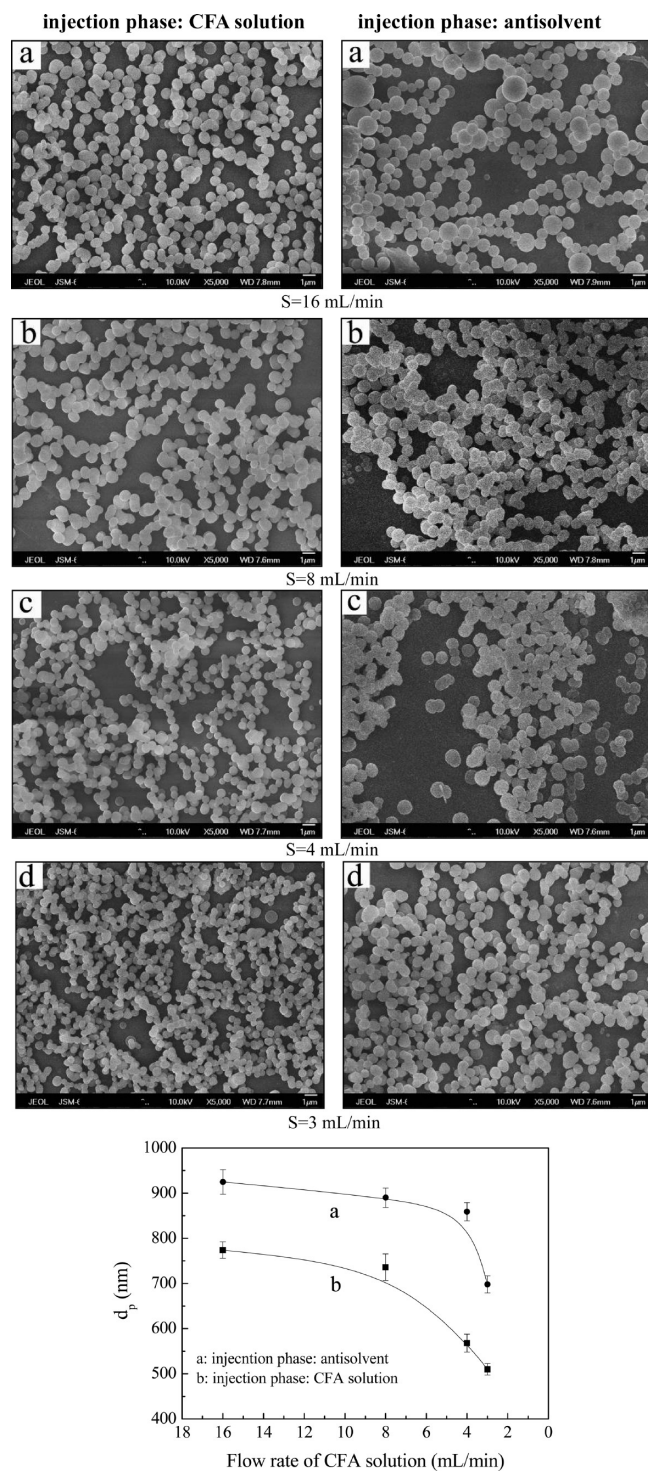


Figure 3. SEM images of CFA nanoparticles obtained at different flow rates of CFA solution by changing the injection phase and corresponding variations of average particle size with the flow rate.

was fixed on an SEM stub using double-sided adhesive tape and coated with Pt at 20 mA for 2 min through a sputter-coater before observation. The particle size distributions were tested by laser diffractometer (Malvern, Zetasizer-3000HS).

An FTIR spectrometer (Nicolet, FTIR-8700) was used to record the FTIR spectrum of the CFA particles in the range of 400–4000 cm⁻¹ using a resolution of 4 cm⁻¹ and 16 scans.

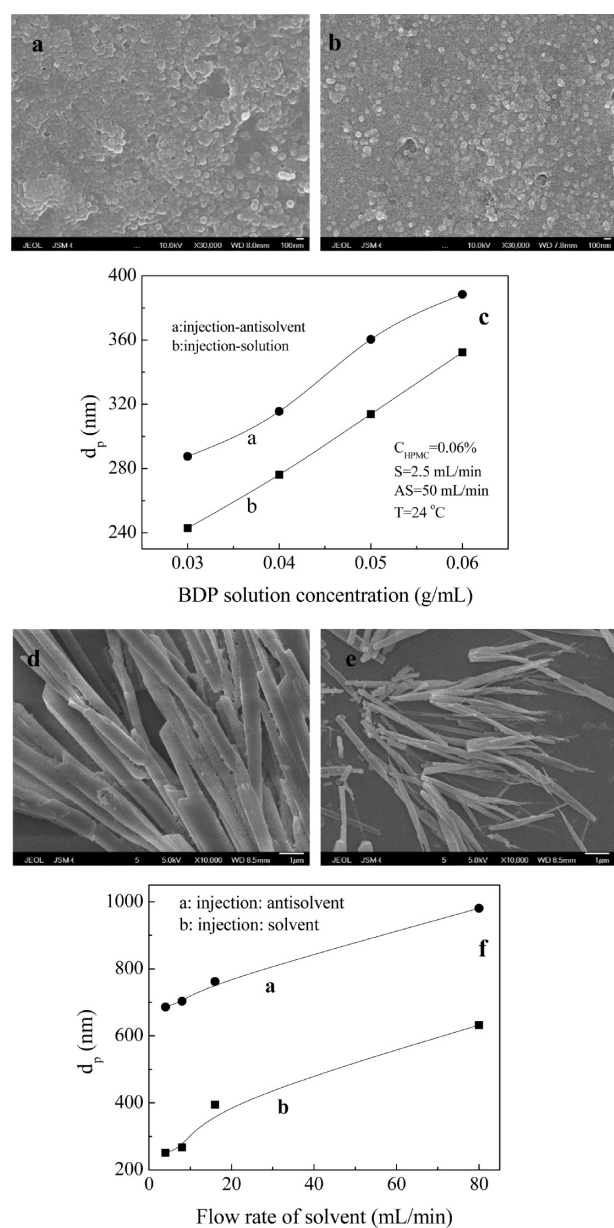


Figure 4. SEM images of BDP particles prepared with and without surfactant in TMC with different injection phases.

Samples were grounded with KBr and pressed into suitable-size disks for measurement.

XRD analysis was performed using a Shimadzu XRD-6000 X-ray diffractometer to detect any change of the physical characteristics and crystallinity. The measuring unit consisted of a rotating anode in transmission mode and used Cu K α radiation generated at 30 mA and 40 kV. Samples were scanned at a rate of 0.05°/min from 5° to 50°.

DSC thermograms of the samples were obtained on a Pyris 1 thermal analysis system (Perkin-Elmer). Samples were heated from 30 to 200 °C at a rate of 10 °C/min in a N₂ atmosphere.

Dissolution tests were performed using a dissolution apparatus (D-800LS, Tianjin) following the USP Apparatus II (paddle) method. The rotation speed of the paddle and the bath temperature were set at 100 rpm and (37.0 ± 0.5) °C, respectively. Approximately 20 mg of drug powder was put into a vessel

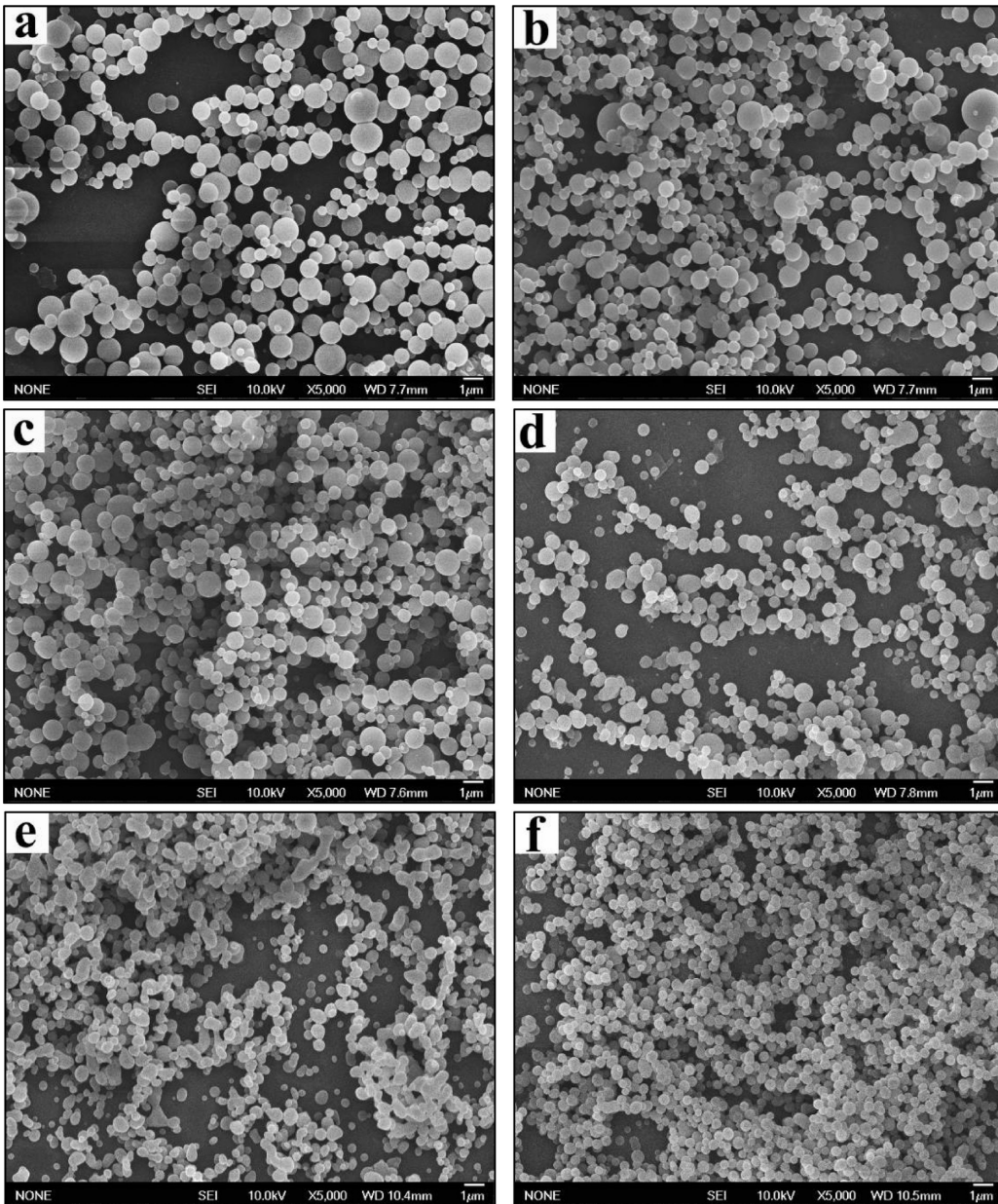


Figure 5. SEM images of CFA particles prepared at different antisolvent flow rates: (a) 30, (b) 40, (c) 50, (d) 60, (e) 70, and (f) 80 mL/min. The solvent flow rate was set at 4 mL/min.

containing 900 mL of 0.1 mol/L HCl solution containing 0.1% (w/v) sodium dodecyl sulfate (SDS). At specific intervals, a sample (5 mL) was withdrawn, filtered through a 0.22- μm syringe filter, and directly injected into a high-performance liquid chromatography system to detect the concentration of the filtrate.

The chromatographic separation was completed using a Waters Sunfire C18, reverse-phase column (150 mm \times 4.6 mm i.d., 5- μm particle size) protected by a guard column (10 mm \times 4.6 mm i.d.) that was packed with the same Sunfire C18 material. The mobile phase was a mixture of methanol and 0.2 mol/L NH₄H₂PO₄ solution (600:400, v/v). The column was maintained at 25 °C and was equilibrated for 40 min with the mobile phase before injection. The injection volume was 50 μL , and the mobile phase was pumped at a flow rate of 1.0 mL/min. The detection wavelength was 278 nm.

The standard curve, given by

$$y = 2.52 \times 10^6 x + 9799.94 \quad (1)$$

where y is the peak area and x is the content of CFA (μg), was linear ($r^2 = 0.9999$) in the range from 0.05 to 1.068 μg .

3. RESULTS AND DISCUSSION

3.1. Effect of Injection Phase on the Size of CFA Particles. Because the microchannel system presented in this work contained a main microchannel and a branch, the selection of the injection phase (the entrance of CFA acetone solution through a branch or a main microchannel) had a great effect on the mixing behavior and flow patterns of the antisolvent and drug organic solution, as well as the subsequently formed CFA nanoparticles.

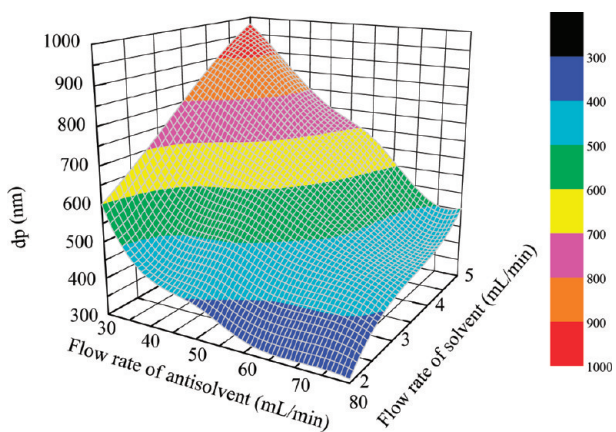


Figure 6. Effect of the antisolvent flow rate on the average particle size, d_p .

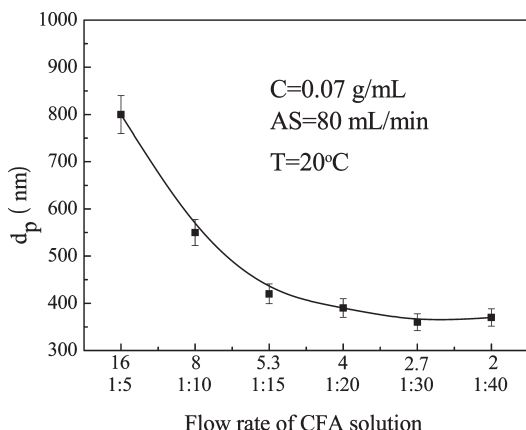


Figure 7. Effect of the CFA acetone solution flow rate on the average particle size, d_p .

Figure 2 shows schematic diagrams for the formation process of CFA nanoparticles in TMC with different injection phases. Figure 3 presents SEM images of CFA nanoparticles obtained under different flow rates of CFA solution at a fixed antisolvent flow rate by changing the injection phase and the corresponding variation of average particle size with the flow rate. Obviously, regardless of whether the CFA acetone solution or the antisolvent was the injection phase, the precipitated CFA particles exhibited first a slow reduction and then a rapid decrease in average particle size from 920 (770) nm to 700 (510) nm, as well as a narrower particle size distribution (PSD) with a decrease in the flow rate from 16 to 3 mL/min. This can be mainly attributed to the rapid increase of the system supersaturation level owing to the increase of the AS/S ratio from 5 to 26.7. More importantly, when the injection phase was CFA acetone solution, the CFA nanoparticles obtained at a given flow rate had a smaller size (curve b) than those obtained when the injection phase was the antisolvent (curve a). The size difference was 150–320 nm. Moreover, a similar phenomenon could also be seen in another investigated drug system, namely, beclomethasone dipropionate (BDP), a member of the inhaled glucocorticosteroid class (see Figure 4). Regardless of whether surfactant was added in the BDP preparation process, obviously smaller (about 50-nm difference) spherical BDP particles or shorter-width (about 400-nm difference) rodlike BDP particles were obtained when

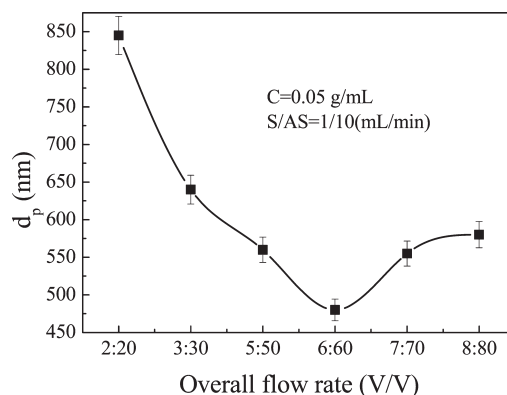


Figure 8. Effect of the overall flow rate on the average particle size, d_p .

the drug solution (solvent), at low flow rate, was selected as the injection phase. Although the reason is not clear, it is reasonable to consider that the local supersaturation could be induced by a variation of local mass-transfer rate due to a change of the local flow velocity field. The detailed reason for these results needs to be further investigated. Therefore, the CFA solution was selected as the injection phase in the subsequent investigations.

3.2. Effect of Liquid Flow Rate on the Size of CFA Particles.

Figures 5 and 6 show SEM images of CFA particles prepared at different antisolvent flow rates and the variation of the average size with antisolvent flow rate. It can be clearly seen that the mean diameters of the CFA particles decreased and the particles became more uniform as the antisolvent flow rate increased. Actually, for a given CFA solution flow rate, increasing the antisolvent flow rate directly led to a large increase of the AS/S ratio, thereby generating a higher supersaturation level. On the other hand, solvent transfer from the CFA acetone solution was enhanced by increasing the Reynolds number (Re), which accelerated the formation of local concentrated zones within the CFA slug regions. These factors are mainly responsible for the formation of smaller CFA particles with narrower PSDs.^{42,45–48}

Figure 7 shows the effect of the CFA acetone solution flow rate on the average particle size. With a decrease in CFA solution rate from 16 to 4 mL/min, the mean diameter sharply decreased, and then it slightly decreased with a further decrease from 4 to 2 mL/min. Clearly, for a given antisolvent flow rate of 80 mL/min, a decrease in the CFA solution rate caused an increase of the AS/S ratio and a higher supersaturation level. In addition, an increase of the relative rates of the flow streams also induced an increase of the mass-transfer rate of solvent. Thus, a decrease in particle diameter was observed.⁴²

Figure 8 presents the variation of the overall flow rate of antisolvent and CFA acetone solution at a fixed AS/S ratio of 10 (v/v). There was a minimum in the average size at an overall flow rate of 66 mL/min. For low overall flow rate (<66 mL/min in this work), the size decrease could be explained by the intensification of the mixing of solvent and antisolvent at increasing overall flow rate. In this case, the CFA acetone solution diffused more rapidly into the antisolvent at a higher flow rate. A uniform spatial concentration distribution could be achieved at the molecular scale, and the creation of smaller local supersaturation zones could be accelerated. These effects were beneficial to the formation of smaller particles with a narrower PSD. However, when the overall flow rate exceeded 66 mL/min, the particle size increased slightly. On the other hand, the incomplete mixing induced at a higher flow rate would result in a nonuniform local supersaturation,

thereby generating larger particles with a wider size distribution. Therefore, it is obvious that the mixing of solvent and antisolvent is crucial to the formation of smaller CFA nanoparticles in the TMC. Once complete mixing or the required residence time is ensured, an increase of the flow rate will be beneficial to the preparation of smaller particles.

3.3. Effect of CFA Solution Concentration on the Size of CFA Particles. Figure 9 shows the effect of the CFA solution concentration on the average size of CFA particles. Clearly, increasing the CFA concentration from 0.06 to 0.09 g/mL decreased the particle size. This result can be attributed to the fact that the nucleation rate is more dependent on the supersaturation level than the crystal growth rate, thereby greatly affecting the final particle size.⁴⁹ A higher drug concentration will create a higher supersaturation level and a higher nucleation rate, benefiting the formation of smaller particles.

3.4. Powder Characterization. Figure 10 shows SEM images of raw CFA and CFA nanoparticles. It can be seen that the CFA nanoparticles precipitated in the TMC (at a solution flow rate of 4 mL/min, an antisolvent flow rate of 80 mL/min, a solution concentration of 0.5 g/mL, and a temperature of 5 °C) had a uniform spherical shape, a good dispersity, and an average particle size of about 300 nm (Figure 10b), whereas raw CFA exhibited a rodlike shape with a length of 2–50 μm (Figure 10a).

Figure 11 shows FTIR spectra of raw CFA and CFA nanoparticles. The FTIR spectrum of the precipitated nanoparticles matches well with that of raw CFA. This demonstrates that the chemical structure of the drug was not changed by the precipitation process. Figure 12 compares the powder XRD patterns of

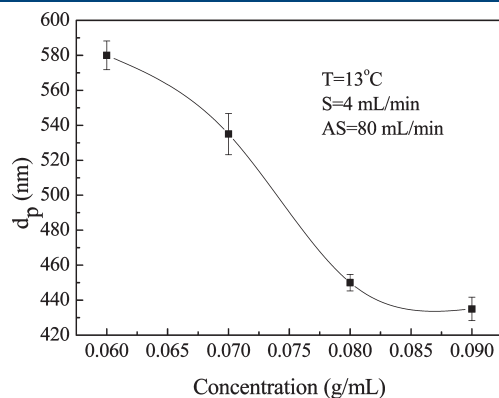


Figure 9. Effect of the CFA concentration on the average particle size, d_p .

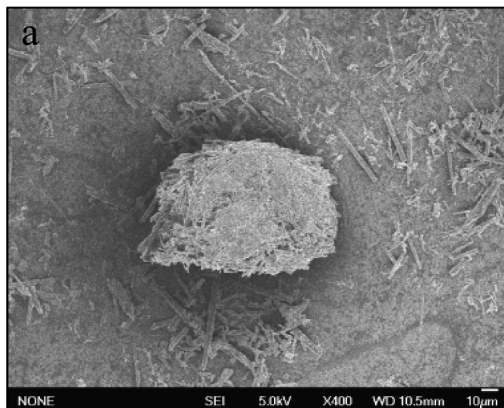


Figure 10. SEM images of raw CFA and CFA nanoparticles.

CFA nanoparticles and raw CFA. It can be clearly seen that the raw CFA is highly crystallized and has intense crystalline peaks between 5° and 50°. However, instead of intense crystalline peaks, CFA nanoparticles produced a halo pattern typical of an amorphous material, where the broad and diffuse maxima were caused by a random arrangement of the constituent molecules. This confirmed that the precipitated CFA power was in a completely amorphous form.

The physical states of raw CFA and CFA nanoparticles were further examined by DSC, with the thermograms shown in Figure 13. The DSC scan of raw CFA showed two endothermic peaks at 129 and 181 °C, confirming that raw CFA was not only

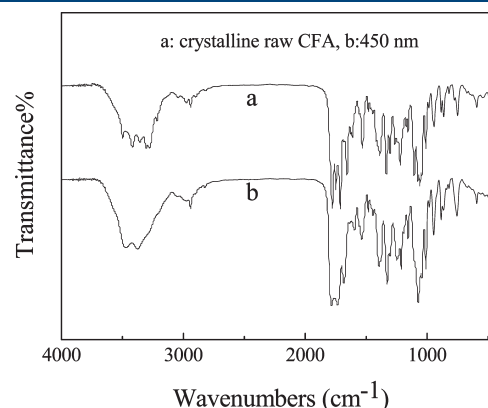


Figure 11. FTIR spectra of raw CFA and 450-nm CFA nanoparticles.

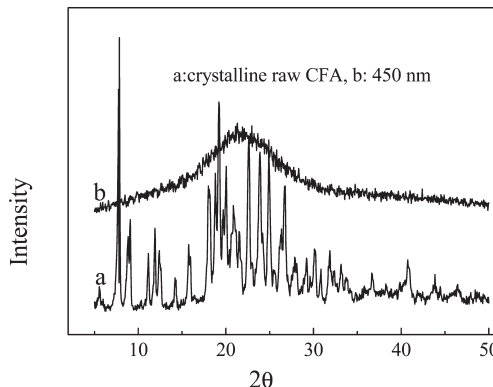
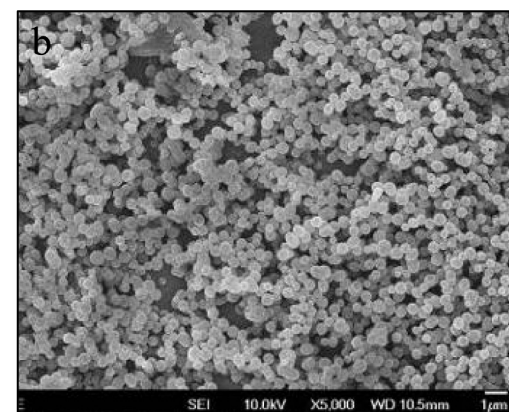


Figure 12. XRD patterns of raw CFA and 450-nm CFA nanoparticles.



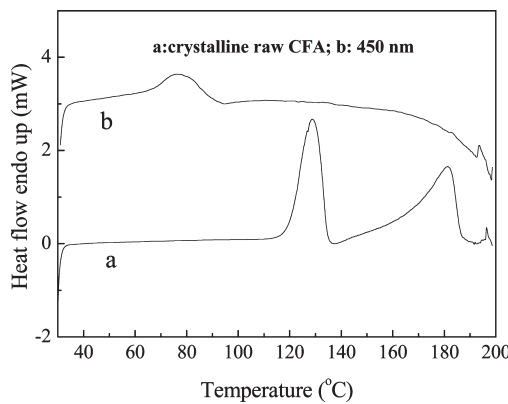


Figure 13. DSC curves of raw CFA and 450-nm CFA nanoparticles.

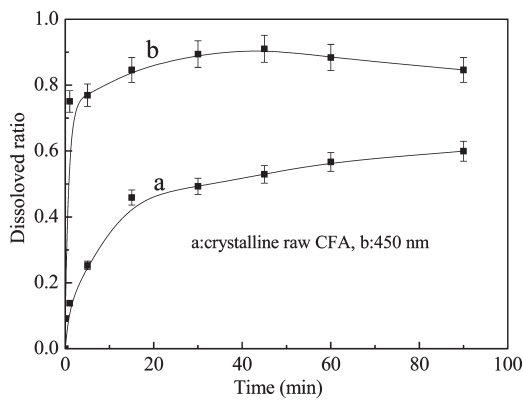


Figure 14. Dissolution rate profiles of raw CFA and 450-nm CFA nanoparticles.

crystalline but also polymorphic. However, only one endothermic band around 80 °C with lower enthalpy appeared in the DSC scans of CFA nanoparticles, indicating that they were in substantially amorphous form.

Figure 14 compares the dissolution profiles of raw CFA and CFA nanoparticles. As expected, compared with raw CFA, CFA nanoparticles with an average size of 450 nm had a significant burst dissolution of 75% in 2 min. During the 90-min testing period, only 55% of the crystalline raw CFA dissolved, whereas about 90% of the CFA nanoparticles were released. The enhanced dissolution of CFA nanoparticles can be mainly ascribed to their amorphous structure and uniform smaller particle size. Moreover, it is well-known that the dissolution rate obeys the Nernst–Noyes–Whitney equation, according to which the dissolution rate can be increased by reducing the particle size at the micro- or nanoscale to increase the specific surface area.^{22,50}

4. CONCLUSIONS

An alternative, effective method using a microchannel system with a T-shaped junction formed by a main microchannel and a branch was presented for nanoprecipitation synthesis of smaller and more homogeneous CFA nanoparticles. In this precipitation process, a change in the injection phase from solvent to antisolvent was found to have a significant effect on the formation of drug nanoparticles. The selection of CFA solution as the injection phase generated more uniform and smaller particles with a narrower PSD. Furthermore, the CFA particle size and PSD

could be controlled by adjusting the operating parameters, such as the flow rates of CFA acetone solution and antisolvent, the overall flow rate, and the CFA concentration. The average drug particle size significantly decreased with a reduction of the CFA solution flow rate, an increase of the antisolvent flow rate, and an increase of CFA solution concentration. However, the particle size and PSD first decreased and then increased with an increase of the overall flow rate. The as-prepared CFA nanoparticles exhibited a great improvement in the dissolution rate compared with raw CFA. Therefore, it is expected that the method described herein should be widely applicable in the preparation of various drug nanoparticles with narrow PSDs.

■ AUTHOR INFORMATION

Corresponding Author

*Tel.: +86-10-64447274. Fax: +86-10-64423474. E-mail: wangjx@mail.buct.edu.cn.

■ ACKNOWLEDGMENT

This work was financially supported by the National Natural Science Foundation of China (Nos. 20806004, 21176013, and 21006002), the National “863” Program of China (No. 2009AA033301), and the Chinese University Scientific Fund (No. JD-1111).

■ REFERENCES

- Chen, X. X.; Lo, C. Y. L.; Sarkari, M.; Williams, R. O., III; Johnston, K. P. Ketoprofen nanoparticle gels formed by evaporative precipitation into aqueous solution. *AICHE J.* **2006**, *52*, 2428–2435.
- Lipinski, C. J. Poor aqueous solubility—An industry wide problem in drug discovery. *Am. Pharm. Rev.* **2002**, *5*, 82–85.
- Müller, R. H.; Jacobs, C.; Kayser, O. Nanosuspensions as particulate drug formulations in therapy: Rationale for development and what we can expect for the future. *Adv. Drug Delivery Rev.* **2001**, *47*, 3–19.
- Perrut, M.; Jung, J.; Leboeuf, F. Enhancement of dissolution rate of poorly soluble active ingredients by supercritical fluid processes. Part I: Micronization of neat particles. *Int. J. Pharm.* **2005**, *288*, 3–10.
- Pathak, P.; Meziani, M. J.; Desai, T.; Sun, Y. P. Nanosizing drug particles in supercritical fluid processing. *J. Am. Chem. Soc.* **2004**, *126*, 10842–10843.
- Raghavan, S. L.; Kiepfer, B.; Davis, A. F.; Kazarian, S. G.; Hadgraft, J. Membrane transport of hydrocortisone acetate from supersaturated solutions; the role of polymers. *Int. J. Pharm.* **2001**, *221*, 95–105.
- Raghavan, S. L.; Schuessel, K.; Davis, A.; Hadgraft, J. Formation and stabilization of tricosan colloidal suspensions using supersaturated systems. *Int. J. Pharm.* **2003**, *261*, 153–158.
- Goddeeris, C.; Coacci, J.; Van den Mooter, G. Correlation between digestion of the lipid phase of smeddls and release of the anti-HIV drug UC 781 and the antimycotic drug enilconazole from smeddls. *Eur. J. Pharm. Biopharm.* **2007**, *66*, 173–181.
- Leuner, C.; Dressman, J. Improving drug solubility for oral delivery using solid dispersions. *Eur. J. Pharm. Biopharm.* **2000**, *50*, 47–60.
- Goddeeris, C.; Willems, T.; Mooter, G. V. D. Formulation of fast disintegrating tablets of ternary solid dispersions consisting of TPGS 1000 and HPMC 2910 or PVPVA 64 to improve the dissolution of the anti-HIV drug UC 871. *Eur. J. Pharm. Sci.* **2008**, *34*, 293–302.
- Tom, J. W.; Debenedetti, P. G. Particle formation with supercritical fluids—A review. *J. Aerosol. Sci.* **1991**, *22*, 555–584.
- Pace, S. N.; Pace, G. W.; Parikh, I.; Mishra, A. K. Injectable formulations of insoluble drugs. *Pharm. Technol.* **1999**, *23*, 116–134.
- Merisko-Liversidge, E.; Iversidge, G. G.; Cooper, E. R. Nanosizing: A formulation approach for poorly-water-soluble compounds. *Eur. J. Pharm. Sci.* **2003**, *18*, 113–120.

- (14) Serajuddin, A. T. M. Solid dispersion of poorly water-soluble drugs: Early promises, subsequent problems, and recent breakthroughs. *J. Pharm. Sci.* **1999**, *88*, 1058–1066.
- (15) Moghimi, S. M.; Hunter, A. C.; Murray, J. C. Long-circulating and target-specific nanoparticles: Theory to practice. *Pharmacol. Rev.* **2001**, *53*, 283–318.
- (16) Hu, J. H.; Johnston, K. P.; Williams, R. O. Nanoparticle engineering processes for enhancing the dissolution rates of poorly water soluble drugs. *Drug Dev. Ind. Pharm.* **2004**, *30*, 233–245.
- (17) Jähnisch, K.; Hessel, V.; Löwe, H.; Baerns, M. Chemistry in microstructured reactors. *Angew. Chem., Int. Ed.* **2004**, *43*, 406–446.
- (18) Wang, K.; Wang, Y. J.; Chen, G. G.; Luo, G. S.; Wang, J. D. Enhancement of mixing and mass transfer performance with a micro-structure minireactor for controllable preparation of CaCO_3 nanoparticles. *Ind. Eng. Chem. Res.* **2007**, *46*, 6092–6098.
- (19) Zhong, J.; Shen, Z. G.; Yang, Y.; Chen, J. F. Preparation and characterization of uniform nanosized cephadrine by combination of reactive precipitation and liquid anti-solvent precipitation under high gravity environment. *Int. J. Pharm.* **2005**, *301*, 286–293.
- (20) Zhao, H.; Wang, J. X.; Wang, Q. A.; Chen, J. F.; Yun, J. Controlled liquid antisolvent precipitation of hydrophobic pharmaceutical nanoparticles in a microchannel reactor. *Ind. Eng. Chem. Res.* **2007**, *46*, 8229–8235.
- (21) Zhao, H.; Wang, J. X.; Zhang, H. X.; Shen, Z. G.; Yun, J.; Chen, J. F. Facile preparation of danazol nanoparticles by high-gravity anti-solvent precipitation method. *Chin. J. Chem. Eng.* **2009**, *17*, 318–323.
- (22) Li, X. S.; Wang, J. X.; Shen, Z. G.; Zhang, P. Y.; Chen, J. F.; Yun, J. Preparation of uniform prednisolone microcrystals by a controlled microprecipitation method. *Int. J. Pharm.* **2007**, *342*, 26–32.
- (23) Pennemann, H.; Hessel, V.; Löwe, H. Chemical microprocess technology—From laboratory-scale to production. *Chem. Eng. Sci.* **2004**, *59*, 4789–4794.
- (24) DeMello, J.; DeMello, A. Microscale reactors: Nanoscale products. *Lab Chip* **2004**, *4*, 11N–15N.
- (25) Song, H.; Chen, D. L.; Ismagilov, R. F. Reactions in droplets in microfluidic channels. *Angew. Chem., Int. Ed.* **2006**, *45*, 7336–7356.
- (26) Sotowa, K. I.; Irie, K.; Fukumori, T.; Kusakabe, K.; Sugiyama, S. Droplet formation by the collision of two aqueous solutions in a microchannel and application to particle synthesis. *Chem. Eng. Technol.* **2007**, *30*, 383–388.
- (27) Zourob, M.; Mohr, S.; Mayes, A. G.; Macaskill, A.; Pérez-Moral, N.; Fielden, P. R.; Goddard, N. J. A micro-reactor for preparing uniform molecularly imprinted polymer beads. *Lab Chip* **2006**, *6*, 296–301.
- (28) Quevedo, E.; Steinbacher, J.; McQuade, D. T. Interfacial polymerization within a simplified microfluidic device: Capturing capsules. *J. Am. Chem. Soc.* **2005**, *127*, 10498–10499.
- (29) Dendukuri, D.; Pregibon, D. C.; Collins, J.; Hatton, T. A.; Doyle, P. Continuous-flow lithography for high-throughput microparticle synthesis. *Nat. Mater.* **2006**, *5*, 365–369.
- (30) Kumemura, M.; Korenaga, T. Quantitative extraction using flowing nano-liter droplet in microfluidic system. *Anal. Chim. Acta* **2006**, *558*, 75–79.
- (31) DeMello, A. J. Control and detection of chemical reactions in microfluidic systems. *Nature* **2006**, *442*, 394–402.
- (32) Poe, S. L.; Cummings, M. A.; Haaf, M. P.; McQuade, D. T. Solving the clogging problem: Precipitate-forming reactions in flow. *Angew. Chem., Int. Ed.* **2006**, *45*, 1544–1548.
- (33) Yen, B. K. H.; Stott, N. E.; Jensen, K. F.; Bawendi, M. G. A continuous-flow microcapillary reactor for the preparation of a size series of CdSe nanocrystals. *Adv. Mater.* **2003**, *15*, 1858–1862.
- (34) Edel, J. B.; Fortt, R.; DeMello, J. C.; DeMello, A. J. Microfluidic routes to the controlled production of nanoparticles. *Chem. Commun.* **2002**, *2*, 1136–1137.
- (35) Wagner, J.; Kirner, T.; Mayer, G.; Albert, J.; Köhler, J. M. Generation of metal nanoparticles in a microchannel reactor. *Chem. Eng. J.* **2004**, *101*, 251–260.
- (36) Lin, X. Z.; Terepka, A. D.; Yang, H. Synthesis of silver nanoparticles in a continuous flow tubular microreactor. *Nano Lett.* **2004**, *4*, 2227–2232.
- (37) Takagi, M.; Maki, T.; Miyahara, M.; Mae, K. Production of titania nanoparticles by using a new microreactor assembled with same axle dual pipe. *Chem. Eng. J.* **2004**, *101*, 269–276.
- (38) Wang, Z.; Chen, J. F.; Le, Y.; Shen, Z. G.; Yun, J. Preparation of ultrafine beclomethasone dipropionate drug powder by antisolvent precipitation. *Ind. Eng. Chem. Res.* **2007**, *46*, 4839–4845.
- (39) Ying, Y.; Chen, G. W.; Zhao, Y. C.; Li, S. L.; Yuan, Q. A high throughput methodology for continuous preparation of monodispersed nanocrystals in microfluidic reactors. *Chem. Eng. J.* **2008**, *135*, 209–215.
- (40) Xu, S. Q.; Nie, Z. H.; Seo, M.; Lewis, P.; Kumacheva, E.; Stone, H. A.; Garstecki, P.; Weibel, D. B.; Gitlin, I.; Whitesides, G. M. Generation of monodisperse particles by using microfluidics: Control over size, shape, and composition. *Angew. Chem., Int. Ed.* **2005**, *44*, 724–728.
- (41) Zhang, S. H.; Shen, S. C.; Chen, Z.; Yun, J. X.; Yao, K. J.; Chen, B. B.; Chen, J. Z. Preparation of solid lipid nanoparticles in co-flowing microchannels. *Chem. Eng. J.* **2008**, *144*, 324–328.
- (42) Karnik, R.; Gu, F.; Basto, P.; Cannizzaro, C.; Dean, L.; Kyei-Manu, W.; Langer, R.; Farokhzad, O. C. Microfluidic platform for controlled synthesis of polymeric nanoparticles. *Nano Lett.* **2008**, *8*, 2906–2912.
- (43) Zhang, H. X.; Wang, J. X.; Shao, L.; Chen, J. F. Microfluidic fabrication of monodisperse pharmaceutical colloidal spheres of atorvastatin calcium with tunable sizes. *Ind. Eng. Chem. Res.* **2010**, *49*, 4156–4161.
- (44) Wang, J. X.; Zhang, Q. X.; Zhou, Y.; Shao, L.; Chen, J. F. Microfluidic synthesis of amorphous cefuroxime axetil nanoparticles with size-dependent and enhanced dissolution rate. *Chem. Eng. J.* **2010**, *162*, 844–851.
- (45) Chen, J. F.; Zheng, C.; Chen, G. T. Interaction of macro- and micromixing on particle size distribution in reactive precipitation. *Chem. Eng. Sci.* **1996**, *51*, 1957–1966.
- (46) Brian, K. J.; Robert, K. P. Chemical processing and micromixing in confined impinging jets. *AIChE J.* **2003**, *49*, 2264–2282.
- (47) Yun, J. X.; Zhang, S. H.; Shen, S. C.; Chen, Z.; Yao, K. J.; Chen, J. Z. Continuous production of solid lipid nanoparticles by liquid flow-focusing and gas displacing method in microchannels. *Chem. Eng. Sci.* **2009**, *64*, 4115–4122.
- (48) Dirksen, J. A.; Ring, T. A. Fundamentals of crystallization: Kinetic effects on particle size distributions and morphology. *Chem. Eng. Sci.* **1991**, *46*, 2389–2427.
- (49) Chen, J. F.; Zhou, M. Y.; Shao, L.; Wang, Y. Y.; Yun, J.; Chew, N. Y. K.; Chan, H. K. Feasibility of preparing nanodrugs by high-gravity reactive precipitation. *Int. J. Pharm.* **2004**, *269*, 267–274.
- (50) Douroumis, D.; Fahr, A. Nano- and micro-particulate formulations of poorly water-soluble drugs by using a novel optimized technique. *Eur. J. Pharm. Biopharm.* **2006**, *63*, 173–175.